On the Structure of Water–Alcohol and Ammonia–Alcohol Protonated Clusters

Z. Karpas,* G. A. Eiceman, C. S. Harden,† and R. G. Ewing
Department of Chemistry, New Mexico State University, Las Cruces, New Mexico, USA

Collision-induced dissociation (CID) of protonated ammonia–alcohol and water–alcohol heteroclusters was studied using a triple quadrupole mass spectrometer with a corona discharge atmospheric pressure ionization source. CID results suggested that the ammonia–alcohol clusters had NH_4^+ at the core of the cluster and that hydrogen-bonded alcohol molecules solvated this central ion. In contrast, CID results in water–alcohol clusters showed that water loss was strongly favored over alcohol loss and that there was a preference for the charge to reside on an alcohol molecule. The results also indicated that a loose chain of hydrogen-bonded molecules was formed in the water–alcohol clusters and that there appeared to be no rigid protonation site or a fixed central ion. *(J Am Soc Mass Spectrom 1993, 4, 507–512)*

Clusters are formed when alcohol vapors are admitted into a high-pressure or atmospheric pressure ionization (API) source [1–17]. The presence of water or ammonia vapors leads to formation of alcohol–water or alcohol–ammonia protonated heteroclusters. Kebarle and co-workers [1, 2] were the first to study water–methanol heteroclusters and proposed that methanol uptake was favored over water uptake for small clusters (with up to six ligands) but that larger clusters could preferentially uptake water. This conclusion was supported by Stace and co-workers [3, 4]. With regard to the nature of the ion at the center of the cluster, Kebarle et al. [1] proposed that the structure could be best represented by $M_{m-1}W_{n-m}CH_3OH_2^+$ (W = water, M = methanol; i.e., the charge preferably resides on a methanol moiety). In contrast, Stace and co-workers [3, 4] proposed a central ion of the type $(CH_3OH)_3H^+$ for the heteroclusters. Thus, the structure of alcohol–water clusters and the site of protonation have been the subject of many investigations [1–17] and some confusion and controversy. Two major structural models have been proposed. In one model, recently proposed by Garvey and co-workers [14], a hydronium (H_3O^+) is placed at the core of the cluster and is solvated by hydrogen-bonded alcohol molecules. This structure is considered to be quite rigid because the solvent molecules may fuse together to form five-membered rings [14]. The other model was proposed by Mautner and co-workers [10–13] and by Graul and Squires [5]. In this model, the solvent molecules form a loose chain of hydrogen-bonded ligands with methanol near the charged centers and water molecules in the periphery. This model is not quite in accordance with that of Kebarle and co-workers [1, 2] and Stace and co-workers [3, 4] but is not totally in contrast with them. In a recent collision-induced dissociation (CID) study, Szulejko et al. [9] suggested that $X_3 \cdot H_2O \cdot H^+$ cluster ions [X = $(CH_3)_2CO$, $(CD_3)CO$, or CH_3OH] had a "linear" structure, with the water at one end of the chain. This was based on the observed loss of the water molecule in CID. In contrast, only acetone was lost from the $[(CH_3)_2CO]_3 \cdot NH_3 \cdot H^+$ cluster, indicating that the cluster contained a central NH_4^+ ion.

An unexpected phenomenon was observed during a study of the mechanism of formation and dissociation of water–alcohol heteroclusters in our laboratory [18]. Clusters of the type $(ROH)_n \cdot H_2O \cdot H^+$ (where R = CH_3, C_2H_5, or C_3H_7), formed in an open API source, exhibited different CID patterns on different occasions when injected into a collision chamber containing argon. Further investigation showed that the presence of traces of ammonia in the supporting gas of the API source was responsible for this.

Ammonia ions were reported to readily cluster with polar molecules, such as acetone [9], trimethylamine [19a], and NH_3 [20]. Ammonia may also cluster with alcohol molecules, forming ions of the type $(ROH)_n \cdot NH_3 \cdot H^+$, separated by only 1 u from the analogous ROH clusters with water.

In the present work, we report and compare the CID patterns of $(ROH)_n \cdot H_2O \cdot H^+$ and $(ROH)_n \cdot NH_3$

* Permanent address: Chemistry Department, Nuclear Research Center, Negev, Beer-Sheva, Israel 84190.
† Permanent address: US Army Chemical Research, Development and Engineering Center, Aberdeen Proving Ground, MD 21010.
Address reprint requests to Zeev Karpas, Department of Chemistry, New Mexico State University, Box 30001, Department 3C, Las Cruces, NM 88003-0001.

1044-0305/93/$6.00

Received September 25, 1992
Revised January 25, 1993
Accepted January 25, 1993

· H^+ clusters and draw inferences about the nature of the central ion in these clusters.

Experimental

All of the measurements reported in this work were completed using a Sciex (Toronto, Canada) TAGA-6000 tandem mass spectrometer, equipped with a corona discharge ion source at ambient pressure (Figure 1). The instrument and operating procedures have been described in detail elsewhere [18, 21] and are only briefly discussed here.

A stream of pure nitrogen provides the plenum gas curtain, separating the API source from the vacuum region in which the mass spectrometers operate. This nitrogen stream could be bubbled through alcohol, water, or water–alcohol solutions, thus introducing vapors from the solution into the plenum. Typically, concentrations of 50–200 ppm of water and/or alcohol vapors were present in the nitrogen plenum gas. Ammonia vapors were introduced into the corona discharge region through a glass tube inlet, either from ambient laboratory air or from a diffusion tube containing NH_4OH.

The electrostatic potentials placed on the ion extraction and focusing lenses impart kinetic energy to the ions and therefore affect the CID patterns. It was found that although cluster size distribution and branching ratios of daughter ions changed with variation of the lense potentials, the effects were quantitative [18]. Dissociation channels were not created or eliminated by changing these potentials over quite a broad range. Unless otherwise indicated, the CID spectra were obtained with potential settings on the ion lenses of OR = 70 V, L2 = 50 V, L3 = 50 V, L4 = 46 V and quadrupole rod settings of R1 = 30 V, R2 = 35 V, and R3 = 35 V. Qualitatively similar CID results were obtained with OR = L2 = L3 = L4 = 50 V, R1 = 43 V, and R2 = R3 = 40 V. As shown by Dawson et al. [21a], the collision energy of ions is determined by the difference between the source potential (taken as the median of OR and L2 voltages) and the DC rod offset of the second quadrupole (R2). When OR and L2 differ, there is some uncertainly in determining the exact source potential [21a]. In the present work, the lowest laboratory collision energy used was therefore 10 V and the highest approximately 25 V. In their experiment with dimethylmorpholinophosphoramidate parent ions with nitrogen target gas, Dawson et al. [21a] found that the center-of-mass collision energy was approximately one-eighth of the laboratory collision energy. The potential difference between OR and L2 strongly affects the dissociation of ions as they go through the plenum gas curtain.

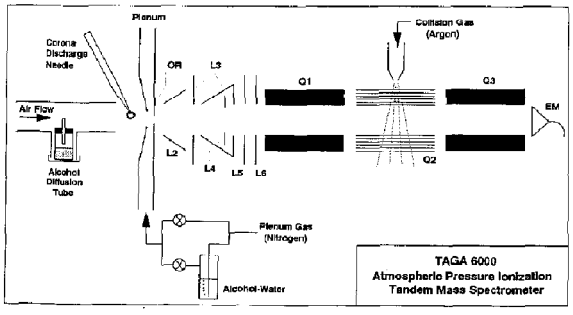

Figure 1. TAGA-6000 API triple quadrupole mass spectrometer (Sciex).

Simple mass spectra were obtained through mass scans on the first quadrupole (Q1) or with the third quadrupole (Q3). When tandem mass spectrometry studies were made, argon was introduced into the region of the second quadrupole (Q2), creating an effective media for CID of the parent ion selected by Q1. The daughter ions formed through these collisions and the undissociated parent ions were then mass analyzed by Q3. The effective thickness of the collision gas is proportional to the total gas pressure in the system. Typically, under the conditions used in the present studies, the background pressure was $2–3 \times 10^{-6}$ torr, corresponding to collision gas thickness (CGT) values of $10–15 \times 10^{12}$ molecules/cm^2. The total pressure with the CID gas was $7–40 \times 10^{-6}$ torr (CGT $1–4.5 \times 10^{14}$ molecules/cm^2). Thus, the total pressure in CID experiments was mainly due to the argon introduced into Q2.

Results and Discussion

Part of a typical corona discharge API mass spectrum, with a mixture of methanol and water vapors in the nitrogen plenum gas, in the presence of ammonia traces, is shown in Figure 2. The main features are the two series of peaks due to methanol clusters $(CH_3OH)_n \cdot H^+$ (denoted **a**) and water–methanol heteroclusters $(CH_3OH)_n \cdot H_2O \cdot H^+$ (denoted **b**). On closer scrutiny, pairs of adjacent peaks were observed, for example, at m/z 50 and 51 u, which were due to a protonated ammonia–methanol $CH_3OH \cdot NH_3 \cdot H^+$ cluster and a water–methanol $CH_3OH \cdot H_2O \cdot H^+$ cluster, respectively. Similarly, several other pairs of adjacent peaks were observed for cluster ions with a different number of methanol molecules.

CID spectra of the ions $(CH_3OH)_2 \cdot NH_3 \cdot H^+$ (m/z 82 u) and $(CH_3OH)_2 \cdot H_2O \cdot H^+$ (m/z 83 u) are shown in Figure 3. There is a marked difference between the two CID spectra. In $(CH_3OH)_2 \cdot NH_3 \cdot H^+$, the only dissociation channels were loss of one or two methanol molecules, as shown in reactions 1a and 1b, respectively:

$$(CH_3OH)_2 \cdot NH_3 \cdot H^+ \rightarrow CH_3OH \cdot NH_3 \cdot H^+ + CH_3OH \quad (1a)$$

$$(CH_3OH)_2 \cdot NH_3 \cdot H^+ \rightarrow NH_4^+ + 2CH_3OH \quad (1b)$$

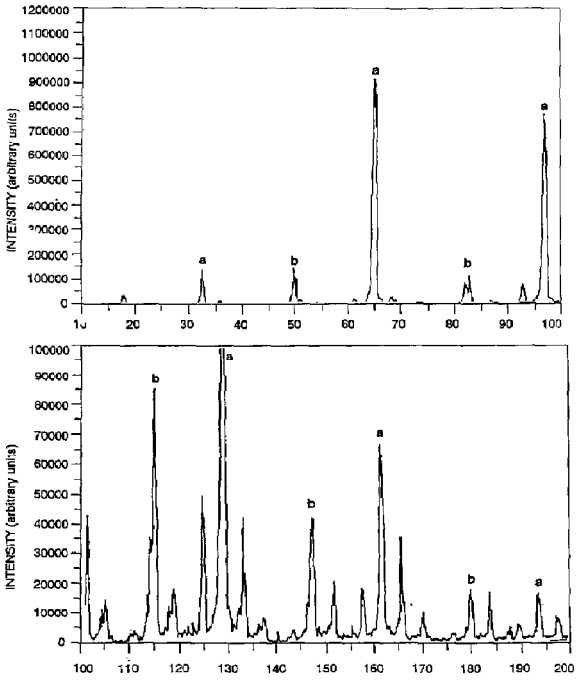

Figure 2. Part of a typical corona discharge API mass spectrum with a mixture of methanol and water vapors in the nitrogen plenum gas, in the presence of ammonia traces. Peaks denoted a were due to $(CH_3OH)_n \cdot H^+$; peaks denoted b were due to $(CH_3OH)_n \cdot H_2O \cdot H^+$ ions.

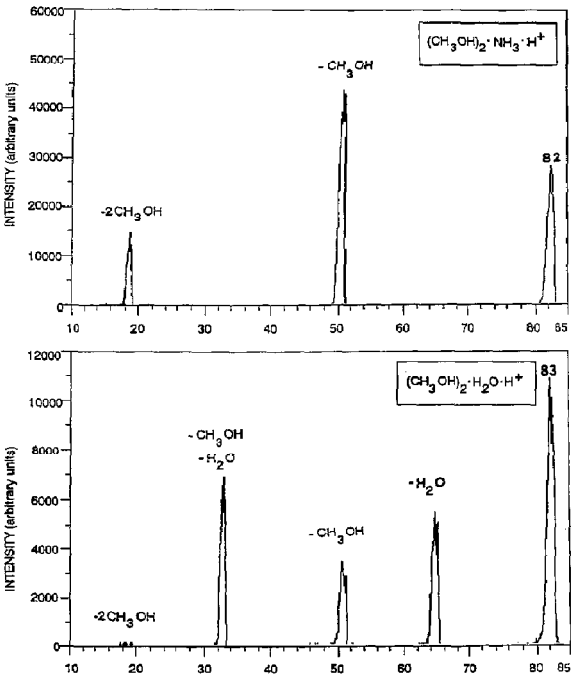

Figure 3. CID spectrum of $(CH_3OH)_2 \cdot NH_3 \cdot H^+$ (m/z 82) and $(CH_3OH)_2 \cdot H_2O \cdot H^+$ (m/z 83).

As seen in Figure 4b and d, the relative intensities of the daughter ions were strongly dependent on the thickness of the argon gas in the collision chamber and on the kinetic energy imparted to the ions by the electrostatic potentials on the ion lenses. On the other hand, the CID spectra of $(CH_3OH)_2 \cdot H_2O \cdot H^+$ showed that loss of water was favored over loss of methanol (reactions 2a and 2b), respectively (Figure 4a and c):

$$(CH_3OH)_2 \cdot H_2O \cdot H^+ \rightarrow (CH_3OH)_2 \cdot H^+ + H_2O \quad (2a)$$

$$(CH_3OH)_2 \cdot H_2O \cdot H^+ \rightarrow CH_3OH \cdot H_2O \cdot H^+ + CH_3OH \quad (2b)$$

Loss of water and methanol (reaction 2c) was also observed as major channel, whereas loss of two methanol molecules (reaction 2d) was unfavored:

$$(CH_3OH)_2 \cdot H_2O \cdot H^+ \rightarrow CH_3OH_2^+ + H_2O + CH_3OH \quad (2c)$$

$$(CH_3OH)_2 \cdot H_2O \cdot H^+ \rightarrow H_3O^+ + 2CH_3OH \quad (2d)$$

As seen in Figure 4a, c, the branching ratio once again depended on the collision gas thickness and electrostatic potentials of the ion lenses.

The CID spectra of larger clusters of methanol with ammonia and water showed similar trends: loss of methanol molecules from the ammonia clusters and loss of water with one or several methanol molecules as the major dissociation channel in the water–methanol clusters. In the larger $(CH_3OH)_n \cdot H_2O \cdot H^+$

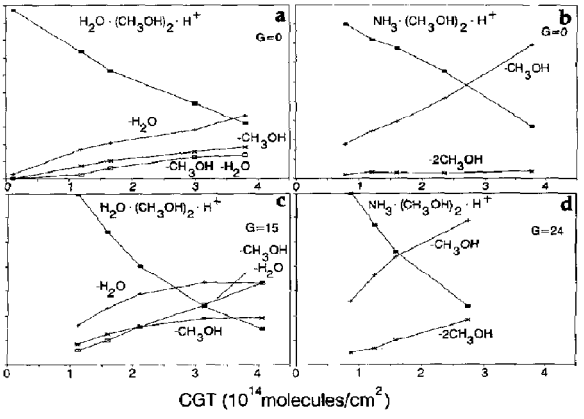

Figure 4. Fraction of parent and daughter ions in the CID spectra of $(CH_3OH)_2 \cdot H_2O \cdot H^+$ and $(CH_3OH)_2 \cdot NH_3 \cdot H^+$ as a function of the collision gas thickness (CGT) at two ion lens potential gradients (G) between OR and L4, with laboratory collision energies, of 10 V (**a**, **b**), 17.5 V (**c**), and 25 V (**d**).

clusters, retention of the water molecule and loss of methanol molecues in the daughter ions were observed in the CID spectrum; however, this was a relatively minor channel, compared with loss of water. Similar results were observed for clusters of ethanol and 2-propanol containing one water molecule or one ammonia molecule. For example, the CID spectra of $(C_3H_7OH)_3 \cdot NH_3 \cdot H^+$ (m/z 198) and of $(C_3H_7OH)_3 \cdot H_2O \cdot H^+$ (m/z 199) are shown in Figure 5a. Loss of propanol molecules and retention of ammonia ion in the daughter ions were observed in the CID spectrum of the former (peaks denoted **a** in Figure 5, top). In the CID spectrum of the latter, the dissociation channels in which loss of the water molecule occurred (denoted **b** in Figure 5, bottom) predominated over dissociation channels in which the daughter ions retained the water (denoted **a** in Figure 5, bottom). It should be noted that due to limitations of resolving power of Q1, there may be some contribution from ions of adjacent mass to these CID spectra. Therefore the peaks denoted **a** in Figure 5 (bottom) may be partly due to impurity $(C_3H_7OH)_3 \cdot NH_3 \cdot H^+$ ions entering the collision chamber with the mass-selected $(C_3H_7OH)_3 \cdot H_2O \cdot H^+$ ions.

The branching ratio between channels in which the daughter ions retained the water molecule and channels in which the water was lost from the daughter ions is summarized in Table 1. On the whole, production of daughter ions that have lost the water molecule was favored over retention of water by a factor of 2 to 4. A general trend of increase in the fraction of daughter ions from which water is lost as the collision gas pressure was increased was also observed.

The stability of heteroclusters toward CID may be estimated from the fraction of parent ions P that survive intact when injected into a chamber containing an inert gas as a function of the thickness of the collision gas in the chamber. Plotting $\ln(P/T)$, where T is the sum of the parent ions and all daughter ions in the CID spectrum, as a function of the collision gas thickness yielded a straight line, the slope of which was inversely proportional to ion stability. In Figure 6, such plots for $(CH_3OH)_2 \cdot H_2O \cdot H^+$ and $(CH_3OH)_2 \cdot NH_3 \cdot H^+$ for two different settings of the ion lens potentials are shown. The effect of increasing the potential gradient on the dissociation rates of two of the clusters is clearly seen here.

Figure 7 depicts the relative dissociation rates (slopes) for the two series of ions $(CH_3OH)_n \cdot H_2O \cdot H^+$ (solid triangles) and $(CH_3OH)_n \cdot NH_3 \cdot H^+$ (open rectangles) as a function of n. The dissociation rates of the ammonia–methanol clusters are slightly higher than those of the corresponding water–methanol clusters. The general trend observed in alcohol clusters is that the rate of dissociation of a cluster ion was proportional to its mass.

The size distribution of ammonia–methanol and protonated methanol clusters derived from the mass spectrum is shown in Figure 8. It should be emphasized that the cluster size distribution shifted as experimental parameters were changed. For example, the

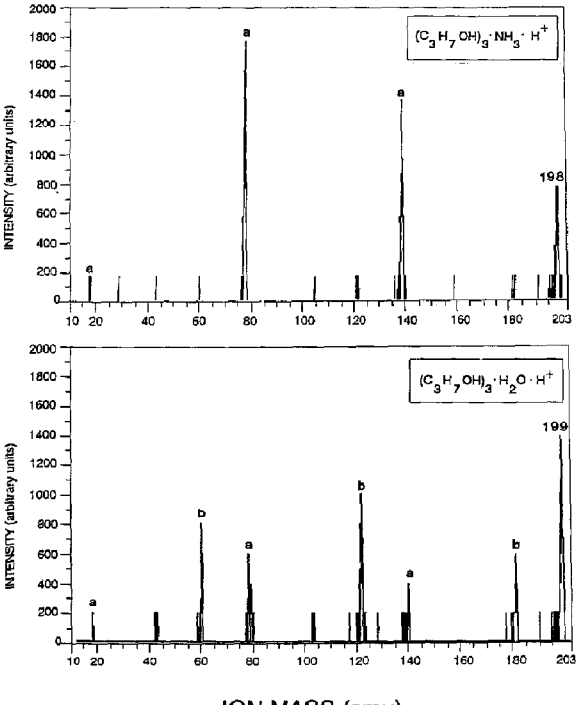

Figure 5. CID spectra of $(C_3H_7OH)_3 \cdot H_2O \cdot H^+$ (m/z 199) and $(C_3H_7OH)_3 \cdot NH_3 \cdot H^+$ (m/z 198): Peaks denoted **a** denote daughter ions in which ammonia or water were retained; peaks denoted **b** denote daughter ions from which water was lost.

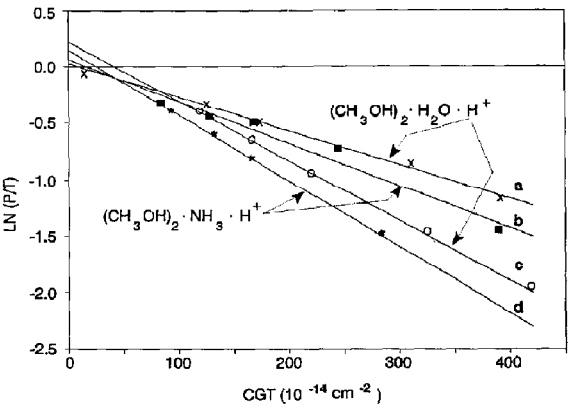

Figure 6. Plot of $\ln(P/T)$, where P is the intensity of parent ions that remained undissociated, and T is the sum of all daughter ions in the CID spectra, as a function of collision gas thickness (CGT): (a, b) OR = L2 = L3 = L4 = 50 V; (c) OR = 60 V, L2 = 55 V, L3 = 50 V, L4 = 45 V; and (d) OR = 70 V, L2 = L3 = 50 V, L4 = 46 V. In all cases, the rod offset potentials were R1 = 43 V and R2 = R3 = 40 V.

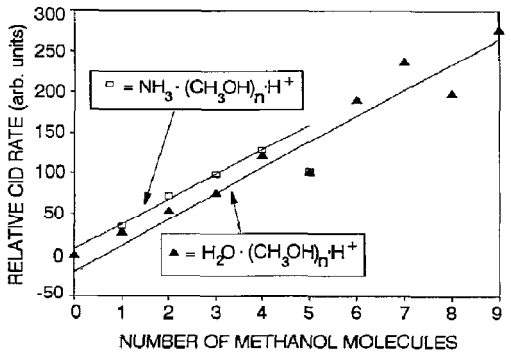

Figure 7. Slope of the dissociation curves for the two series of ions $(CH_3OH)_n \cdot H_2O \cdot H^+$ and $(CH_3OH)_n \cdot NH_3 \cdot H^+$ as a function of n.

composition of the plenum gas and the potential gradient on the ion lenses considerably altered the distribution, as was shown for protonated methanol and methanol water clusters.

The existence of "magic numbers" is not apparent in the cluster size distribution and in the relative stability curves. This result is somewhat surprising because one would expect that the cluster of ammonia with four alcohol molecules would exhibit some enhanced stability [19] owing to the availability of exactly four hydrogen atoms with which the alcohol may form a strong hydrogen bond; however, this is in accordance with Xu et al. [17] who reported that in their experiment, there was a logarithmic decrease in abundance with cluster size in protonated methanol, water–methanol, and dimethyl ether–methanol clusters, whereas "magic numbers" were not found.

On the other hand, "magic numbers" were observed in clusters of ammonia ions with trimethylamine, acetone, acetonitrile, and acetaldehyde [19]. The lack of observation of clusters with abnormal stability in the present work may be due to the conditions in which ions are formed and dissociated. Unlike most other experiments in which neutral clusters are formed

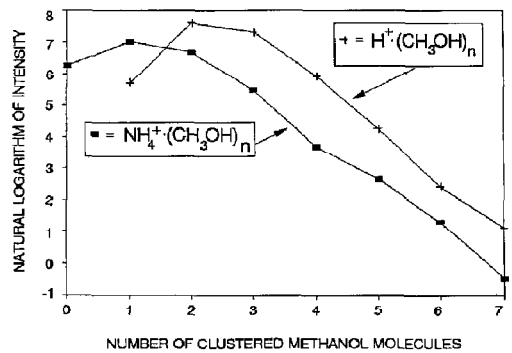

Figure 8. Size distribution of ammonia–methanol and protonated methanol clusters derived from the mass spectrum.

through supersonic (and cooled) expansion of an inert gas beam, which are then ionized, here ions formed in the corona discharge region are introduced into the plenum gas where most of the clustering occurs.

Summary and Conclusions

The CID results presented here yield information on the structure of the protonated water–methanol and ammonia–methanol heteroclusters. Information on the position of the charge (site of protonation) in these clusters may be inferred from the CID results. Evidently, loss of methanol molecules only from the ammonia–methanol clusters indicates that the charge resides on the ammonia moiety. Thus, the structure of these clusters corresponds to that of a central NH_4^+ core ion solvated by methanol molecules. This is analogous to the results of Szulejko et al. [9], who concluded that ammonia–acetone trimers had a central NH_4^+ ion, and in accordance with Castleman and co-workers [19], who found a similar structure for ammonia–trimethylamine clusters.

On the other hand, the CID results demonstrate that the water–methanol clusters do not have a rigid H_3O^+ core ion that is solvated by methanol molecules. From CID results it appears that the charge preferably resides on a methanol molecule. The CID results indicate that the ligands do not form orderly rigid shells but rather a kind of loose hydrogen-bonded chain. Furthermore, when considering the lability of the proton in the cluster, proposing a fixed site of protonation in the water–alcohol clusters is even less viable. These conclusions are in accordance with the model suggested by other workers [1–13] but in contrast with the model presented by Garvey and co-workers [14].

The differences in the proton affinities [22] (PAs) of ammonia, methanol, and water (204.0, 181.9, and 166.5 kcal/mol, respectively) probably influence the structure and stability of the heteroclusters. First, the favored site of protonation in a heterocluster would usually be close to the component with higher proton affinity, with exceptions in cases where this leads to blocking of the cluster growth [23]. Thus, the charge resides on the ammonia moiety in the ammonia–alcohol clusters and close to the alcohol in alcohol–water clusters. Second, generally speaking, the smaller the difference in the PAs of the components of proton-bridged dimers, the more stable is the ion [24]. Thus, for example, symmetric protonated dimers are more stable toward dissociation than asymmetric ones, although the bonding energy in symmetric protonated dimers was shown to decrease with increasing PA [10]. This may explain why ammonia–methanol clusters, where the PA difference between the components is 22.1 kcal/mol, have a larger tendency to dissociate (larger slopes in their CID stability plots) than the corresponding water–methanol clusters, where the PA

Table 1. Percent of daughter ion intensities in which water is retained versus water loss from CID spectra of $(ROH)_n \cdot H_2O \cdot H^+$ parent ions at a total pressure of $7 \pm 1 \times 10^{-6}$ torr

Parent ion	Water retention (%)	Water loss (%)
$(CH_3OH) \cdot H_2O \cdot H^+$	< 5	< 95
$(CH_3OH)_2 \cdot H_2O \cdot H^+$	30	70
$(CH_3OH)_3 \cdot H_2O \cdot H^+$	20	80
$(CH_3OH)_4 \cdot H_2O \cdot H^+$	20	80
$(CH_3OH)_5 \cdot H_2O \cdot H^+$	25	75
$(CH_3OH)_7 \cdot H_2O \cdot H^+$	25	75
$(CH_3OH)_8 \cdot H_2O \cdot H^+$	20	80
$(CH_3OH)_9 \cdot H_2O \cdot H^+$	40	60
$(C_3H_7OH)_3 \cdot H_2O \cdot H^+$	35	65

difference is 15.4 kcal/mol. Taking the more current [25] value of 208 kcal/mol for the PA of ammonia only enhances this effect. An important implication of this is that alcohols with PAs closer to that of ammonia than that of water may form clusters with the former that are more stable than the corresponding clusters with the latter. PA differences may also explain the preference of water–alcohol heteroclusters to lose water rather than alcohol and the high abundance of daughter ion from which water was eliminated (Table 1). The moiety with lower PA (water) has a lower binding energy to the core ion than the species with higher PA (the alcohol), and therefore that bond is more readily cleaved. This is true for small clusters, such as those studied in the present work, where the PA differences are related to those of the gas-phase species. In large clusters, however, the solvation of the central ion may alter the effective forces exerted within the cluster.

Finally, it should be noted that the proximity of protonated ammonia–alcohol and water–alcohol clusters in the mass spectrum and the differences in their dissociation patterns may lead to misinterpretation of CID results and erroneous conclusions with regard to the structure of the clusters.

Acknowledgments

We acknowledge the financial assistance of KRUG Life Sciences under purchase order number 50,016 and the encouragement of Dr. Thomas Limero.

References

1. Kebarle, P.; Haynes, R. N.; Collins, J. G. *J. Am. Chem. Soc.* **1967**, *89*, 5753.
2. Grimsrud, E. P.; Kebarle, P. *J. Am. Chem. Soc.* **1973**, *95*, 7939.
3. Stace, A. J.; Shukla, A. K. *J. Am. Chem. Soc.* **1982**, *104*, 5314.
4. Stace, A. J.; Moore, C. *J. Am. Chem. Soc.* **1983**, *105*, 1814.
5. Graul, S. T.; Squires, R. R. *Int. J. Mass Spectrom. Ion Processes* **1987**, *81*, 183.
6. Castleman, A. W. Jr.; Keesee, R. G. *Acc. Chem. Res.* **1986**, *19*, 413.
7. Morgan, S.; Castleman, A. W. Jr. *J. Am. Chem. Soc.* **1987**, *109*, 2867.
8. (a) Morgan, S.; Castleman, A. W. Jr. *J. Phys. Chem.* **1989**, *93* 4544; (b) Morgan, S.; Keesee, R. G.; Castleman, A. W. Jr. *J. Am. Chem. Soc* **1989**, *111*, 3841.
9. Szulejko, J. E.; Hop, C. E. C. A.; McMahon, T. B.; Harrison, A. G.; Young, A. B.; Stone, J. A. *J. Am. Soc. Mass Spectrom.* **1992**, *3*, 33.
10. Meot-Ner (Mautner), M. *J. Am. Chem. Soc.* **1992**, *114*, 3312.
11. El-Shall, M. S.; Schriver, K. E.; Whetten R. L.; Meot-Ner (Mautner), M. *J. Phys. Chem.* **1989**, *93*, 7969.
12. El-Shall, M. S.; Marks, C.; Sieck, L. W.; Meot-Ner (Mautner) M. *J. Phys. Chem.* **1992**, *96*, 2045.
13. Meot-Ner (Mautner), M. *J. Am. Chem. Soc.* **1986**, *108*, 6189.
14. Herron, W. J.; Coolbaugh, M. T.; Vaidyanathan, G.; Peifer, W. R.; Garvey, J. F. *J. Am. Chem. Soc.* **1992**, *114*, 3684.
15. Hiraoka, K.; Takimoto, H.; Morise, K. *J. Am. Chem. Soc.* **1986**, *108*, 5683.
16. Nishi, N.; Yamamoto, K. *J. Am. Chem. Soc.* **1987**, *109*, 7353.
17. Xu, Y.; Jarvis, V. M.; Bostwick, D. E.; Moran, T. F. *Org. Mass Spectrom.* **1991**, *26*, 892.
18. Karpas, Z.; Eiceman, G. A.; Harden, C. S.; Ewing, R. G. *J. Phys. Chem.*, submitted.
19. (a) Wei, S.; Tzeng, W. B.; Castleman, A. W. Jr. *J. Phys. Chem.* **1991**, *95*, 585; (b) Tzeng, W. B.; Wei, S.; Neyer, D. W.; Keesee, R. G.; Castleman, A. W. Jr. *J. Am. Chem. Soc.* **1990**, *112*, 4097.
20. (a) Garvey, J. F.; Peifer, W. R.; Coolbaugh, M. T. *Acc. Chem. Res.* **1991**, *24*, 48; (b) Peifer, W. R.; Coolbaugh, M. T.; Garvey, J. F. *J. Chem. Phys.* **1989**, *91*, 6684; (c) Buck, U.; Krohne, R.; Linnartz, H. *J. Chem. Phys*, **1990**, *93*, 3726; (d) Hirao, K.; Fujikawa, F.; Konishi, H.; Yamabe, S. *Chem. Phys. Lett.* **1984**, *104*, 184.
21. (a) Dawson, P. H., French J. B.; Buckley, J. A.; Douglas, D. J.; Simmons, D. *Org. Mass Spectrom.* **1982**, *17*, 205; (b) Snyder, A. P.; Harden, C. S. *Org. Mass Spectrom.* **1990**, *25*, 53.
22. Lias, S. G.; Liebman, J. F.; Levin, R. D. *J. Phys. Chem. Ref. Data* **1984**, *13*, 695.
23. El-Shall, S. M.; Daly, G. M.; Gao, J.; Meot-Ner (Mautner), M.; Sieck, L. W. *J. Phys. Chem.* **1992**, *96*, 507.
24. Hagler, A. T.; Karpas, Z.; Klein, F. S. *J. Am. Chem. Soc.* **1979**, *101*, 2191.
25. Meot-Ner (Mautner), M.; Sieck, L. W. *J. Am. Chem. Soc.* **1991**, *112*, 4448.